Springer

KSME

Journal of Mechanical Science and Technology 31 (3) (2017) 1241~1257
www.springerlink.com/content/1738-494x(Print)/1976-3824(Online)
DOI 10.1007/s12206-017-0223-0

Unsteady computation of flow field and convective heat transfer over tandem cylinders at subcritical Reynolds numbers †

S. K. Dhiman[1,*], Arbind Kumar[1] and J. K. Prasad[2]

[1]*Department of Mechanical Engineering, Birla Institute Technology, Mesra, Ranchi, 835215, India*
[2]*Department of Space Engineering and Rocketry, Birla Institute Technology, Mesra, Ranchi, 835215, India*

(Manuscript Received August 8, 2016; Revised October 14, 2016; Accepted October 21, 2016)

Abstract

Unsteady flow and convective heat transfer over single and two tandem cylinders at constant-heat-flux condition in subcritical range of Reynolds number was numerically investigated. Two-dimensional computations were performed by adopting 3-equation k-kl-ω turbulence model using a commercial software FLUENT®. The aim was to investigate the capabilities of k-kl-ω turbulence model for collective flow and heat transport conditions past cylindrical bodies and then to identify a critical spacing ratio for the maximum heat transport. The center-to-center spacing ratio (*L/D*) was varied in the range from 1.2 to 4.0. Instantaneous path lines and vorticity contours were generated to interpret the interaction of shear layer and vortices from upstream cylinder with the downstream cylinder. Comparison of pressure coefficients, fluctuating and average lift as well as drag coefficients, Strouhal number and the local and average Nusselt numbers with the available literatures indicated a reasonably good agreement. The combined outcome of flow field and heat transfer study revealed a critical spacing ratio of *L/D* = 2.2. Based on the present investigation, a correlation has been suggested to calculate overall average Nusselt number of the two cylinders placed in tandem.

Keywords: Unsteady computations; Flow and convective heat transfer; Cylinders; Constant-heat-flux; k-kl-ω turbulence model; Spacing ratio

1. Introduction

In waste-heat recovery equipment, such as cross-flow type recuperator, the air flows over the tube surfaces while hot fluid flows through the tubes. These tubes are usually circular and are arranged in either an in-line or staggered manner. For high heat transfer rates, the air velocity must be high because of its poor thermal conductivity; thus, the Reynolds number occurs in subcritical range, while the heat transfer takes place under unsteady state condition and under constant-heat-flux condition. The instabilities behind the cylinders due to discrepancies in the vortex-shedding phenomenon because of variation in spacing between the tubes and flow velocity makes the problem numerically critical for simultaneous determination of flow and heat transfer parameters as well as correct flow structure around the cylinders. Fluid flow and heat transfer from circular cylinders including tandem arrangement has been splendidly investigated by researchers [1-4]. Some of these investigations are reviewed here.

Several CFD simulations have been reported for flow field and heat transfer around cylinders to establish turbulence models such ask-ε, k-ω and k-ω (SST) [5-8]. Kondjoyan and Boisson [5] confirmed that using the k-ε turbulence model with wall function as near wall treatment has very low capacity to calculate heat transfer, while that with Wolfshtein's low-Reynolds number model as near wall treatment has good ability to calculate heat transfer. They suggested that k-ε turbulence model should be used for CFD calculation instead of heat transfer calculations. Numerical study from a cylinder in cross flow by Szczepanik et al. [6] suggested that the Standard k-ω model as well as SST k-ω model does not accurately predict the heat transfer; however, it predicts close results of flow parameters. Younis et al. [7] solved the problem of prediction of heat transfer with vortex shedding conditions in k-ε turbulence model [5], which was achieved by redefining the coefficient of energy dissipation by viscosity action on small scales. Rahman et al.'s numerical study [8] suggested that the standard k-ε model accurately computes drag coefficients, the realizable k-ε turbulence model is highly suitable for visualization of vortex shedding and the SST k-ω model is highly suitable for flow parameters at high Reynolds numbers.

Mittal et al. [9], Meneghini et al. [10] and Jester and Kallinderis [11] performed numerical investigations based on 2D Finite-element method (FEM) for the flow around a pair of stationary circular cylinders. Simulations of Mittal et al. [9] in

*Corresponding author. Tel.: +91 9430734803, Fax.: +91 651 2275401
E-mail address: sushil_k_dhiman@yahoo.co.in
† Recommended by Associate Editor Donghyun You

tandem arrangement at $Re = 10^2$ and 10^3 depict no vortices formation from upstream cylinder at $Re = 10^2$ although their formation was observed at $Re = 10^3$. The investigation also focused on mean values of drag and lift coefficients and Strouhal number. Meneghini et al. [10] in tandem arrangement at $Re = 10^2$ and $2x10^2$ showed consistency with reported experimental results and depicted a negative drag on the downstream cylinder for $L/D < 3$. For $L/D < 3$ the vortices shed only from the downstream cylinder, and for $L/D \geqslant 3$ they shed from both the cylinders. Simulations of Jester and Kallinderis [11] in tandem arrangement at $Re = 0.8x10^2$ and 10^3 show hysteric effects of fluid forces on the cylinders at $Re = 10^3$ for spacing ratio (L/D) between 2.0-2.5. Carmo et al. [12] reported a secondary vortex street in the wake far behind the downstream cylinder in their computational simulations based on spacing ratio between 1.5 to 5.0 and low Reynolds numbers. The two computational methods related to complex geometries, Lattice gas automata (LGA) and Lattice Boltzmann method (LBM), which are widely used for resolving problems involving combined flow field and heat transfer phenomena, have been described by Jiang et al. [13] and Chen et al. [14]. Jiang et al. [13] used two tandem cylinders of different diameters under unconfined and confined flows, while Chen et al. [14] used a heated stationary circular cylinder. The flow domain and time are discrete in the flow models and have low computational cost. Islam and Zhou [15] did a numerical study on the flow past a row of circular cylinders using Lattice Boltzmann method at $Re = 50$, 100 and 200 by varying the distance between the cylinders to investigate the effect of blockage ratio on the drag coefficient, vortex wake and Strouhal number. Islam et al. [16] performed 2D numerical simulations over four in-line rectangular configurations of square cylinders by using the LBM to study the effect of the spacing between the cylinders, mean drag coefficient, Strouhal number and the r.m.s. value of the drag and lift coefficients.

Unsteady computational study of Juncu [17] on tandem cylinders for $1 \leqslant Re \leqslant 30$ and $0.1 \leqslant Pr \leqslant 100$ showed the influence of ($Re.Pr$) on heat transfer rate, such that a high convection rate, a small gap and high volume heat capacity ratios led to a high heat transfer rate. Numerical study of Mihir and Altac [18] for $2 \leqslant L/D \leqslant 10$ past the tandem cylinders at $Re = 100$ and 200 using FLUENT showed that the mean Nu of upstream cylinder and the single cylinder becomes similar at $L/D \geqslant 4$. Jayawel and Tiwari [19] developed 3D computational code for unsteady laminar flow past single and tandem cylinders based on SIMPLE algorithm and finite volume technique to compare the flow and heat transfer results at $Re = 400$. From numerical study using an overset grid method for $2 \leqslant L/D \leqslant 10$ past two and three tandem cylinders, Harimi and Saghafian [20] developed empirical relations in terms of L/D, Re and Pr to predict mean Nu. Lee et al. [21] performed a numerical study to control pitch distance on a tube bank to enhance heat transfer and have developed a correlation for the Nusselt number in terms of pitch ratio.

Igarashi [22] experimentally investigated the flow around tandem circular cylinders to classify the flow pattern for $0.87x10^4 \leqslant Re \leqslant 5.2x10^4$ and $1.3 \leqslant L/D \leqslant 5$. Formation of quasi-stationary vortices was reported up to $L/D \leqslant 3.5$. Experimental study of Alam et al. [23] at $Re = 6.5x10^4$ for spacing ratio 0.1 to 8 between tandem cylinders showed the sensitiveness of the fluctuating lift (C_{Lf}) and drag (C_{Df}) coefficients of downstream cylinder for the spacing ratios before the critical value of $L/D = 3.0$. The values of C_{Lf} and C_{Df} at $L/D = 1.4$ were about 2 and 2.8 times higher, respectively, as compared to single cylinder. The C_{Lf} of upstream cylinder beyond the critical spacing was strongly influenced by the phase of the flow pattern of the downstream cylinder. The shear layer that separates from the upstream cylinder reattaches on the downstream cylinder steadily for $2 < L/D < 3$ and alternately for $L/D < 2$ that undergoes a super-harmonic frequency of twice the Strouhal frequency. A 3D numerical investigation of Kitagawa and Ohta [24] at $Re = 2.2x10^4$ for the spacing ratio from 2 to 5 between tandem cylinders showed a critical spacing ratio of $L/D = 3.5$, before which the vortices shed only from the downstream cylinder and after which the vortices shed from both the upstream as well as downstream cylinder. However, for $L/D \geqslant 3.5$, the fluctuating lift and drag as well as the pressure coefficients of the downstream cylinder were higher than the experimental values from the other reported literatures.

Kostic and Oka [25] conducted experiments by varying the spacing ratio (L/D) between 1.6 to 9.0 and that the Reynolds number between $1.2x10^4$ to $4x10^4$ showing the proportionality of Nusselt number to $Re^{0.6}$ for the upstream cylinder at all L/D. For the downstream cylinder, they further showed the proportionality of Nu to $Re^{0.6}$ for $L/D \geqslant 2.7$ and to $Re^{2/3}$ at $L/D < 2.7$ for the downstream cylinder. Igarashi and Yamasaki [26] from their experimental investigation at $L/D = 1.3$ and $3.9x10^4 \leqslant Re \leqslant 6.2x10^4$ showed a bistable regime for $2x10^4 \geqslant Re \geqslant 3x10^4$. However, no reattachment was observed for $Re \leqslant 2x10^4$ and a permanent reattachment was observed for $Re \geqslant 3x10^4$. They also concluded that the reattachment considerably improves the local Nusselt number of the downstream cylinder, which results in an overall Nu_{avg} twice that of the upstream cylinder. Buyruk [27] experimentally showed the effect of blockage on the heat transfer from one tube within a bundle of staggered tubes as well as within a row of the tubes.

From an experimental study, Daloglu and Unal [28] showed the effect of circular and square obstacles of different sizes placed before a circular cylinder on heat transfer by varying the spacing ratio (L/D) between 0.8 to 9 and the Reynolds number from $0.11x10^4$ to $1.95x10^4$. Tsutsui and Igarashi [29] experimentally studied the augmentation of heat transfer from a cylinder of diameter (D) by placing a rod before it at different distances by varying the rod diameter (d). They showed a 40 % enhancement of heat transfer at $L/D = 1.25$ and $d/D = 0.25$ for a range of Reynolds number from $1.5x10^4$ to $6.2x10^4$.

Various inverse methods have been used to resolve the difficulties in the expensive measuring processes or the direct measurements. It requires merely the measurement of tem-

perature somewhere below the surface of the cylinder. An inverse method by Lin et al. [30] was based on the linear least-squares-error method which utilizes reverse matrix from the temperature measurements. Coment et al. [31] compared the analytical solution (integral transform) and the conjugate gradient methods based on the inverse heat conduction approach to estimate local heat transfer coefficient on two-dimensional cylinders. Chen et al. [32] combined the reverse matrix method and the linear least-square-error method to estimate the unknown heat flux on thick-walled circular tubes. Chen et al. [33-35] adopted an inverse-heat-conduction technique and studied the effect of spacing between the circular and rectangular fins on the heat transfer coefficient. Taler [36] proposed two inverse methods: (i) A singular value decomposition method and (ii) a Levenberg-Marquardt method. Olsson et al. [37] used an inverse approach by using Monte Carlo simulations for sensitivity analysis to determine heat transfer coefficients around a circular cylinder placed on a flat surface by impinging slot air jet on it. Combining the finite element method with the conjugate gradient algorithm, the heat transfer coefficient was estimated on a circular plane fin by Benmachiche et al. [38]. Chen [39] approached an inverse algorithm constructed on the conjugate gradient method for the estimation of space and time dependent heat flux at the surface of a hot cylinder cooled by a laminar confined slot impinging jet.

From the extensive literature reviews it has been observed that the unsteady convective heat transfer investigations based on cross-flow past the tandem cylinders in subcritical range of Reynolds number have been carried out only experimentally. However, merely flow field investigations under such conditions have been reported experimentally as well as numerically. The available computational heat transfer investigations were conducted at Reynolds number less than 10^3. Many turbulence models have been developed for the predictions of flow and heat transfer data, but unfortunately for the subcritical range of Reynolds number, they do not provide good agreements for the collective flow field and heat transfer data.

The present study is concerned with the unsteady computations in a two-dimensional domain by using a 3-equation k-kl-ω turbulence model to the obtain collective flow field and heat transfer data from a single and the two tandem cylinders subjected to the cross-flow of air. The flow field parameters such as pressure coefficient, fluctuating as well as average lift and drag coefficients and the Strouhal number were obtained, and compared with the available literature. The local, fluctuating and average Nusselt numbers were obtained at the cylinder surfaces, and to verify the numerical scheme used in the present study, they are compared with the available literature for single cylinder in terms of dimensionless parameters normalized with Reynolds number. Instantaneous vorticity contours as well as pathlines were obtained to interpret and discuss the flow behavior and heat transfer of the tandem cylinders. A correlation has been suggested to calculate overall average Nusselt number under constant-heat-flux condition of the two tandem cylinders at the critical spacing ratio obtained by the interpretation of combined flow and heat transport results.

Organization of the paper:

The governing equations and the turbulence model along with the boundary conditions and the computational plan are discussed in Sec. 2. Dimensionless parameters, simulation procedure, results of the grid independence test and the verifications of the numerical scheme are also discussed in Secs. 2.1 and 2.2. Sec. 3 illustrates the results and discussion in which first the results of single cylinder are compared with the available literature. This section proves the validity of the numerical scheme used in the present study on single cylinder. Subsequently, the results of the flow and heat transfer over the two tandem cylinders are discussed.

2. Numerical method and model

For numerical solution of the flow equations, a commercial software FLUENT [55] was employed. FLUENT uses finite volume method and implicit techniques to solve the governing equations which are solved sequentially. In the present computational study, the unsteady characteristics of flow field and heat transfer from the cylinders in cross flow of air were investigated. The governing equations were solved as an incompressible problem by applying a Constant-heat-flux (CHF) condition at the cylinder surface and the turbulent flows were simulated using a k-kl-ω turbulence model.

The governing equations are:

Continuity equation:

$$\left(\frac{\partial \rho}{\partial t}+\frac{\partial(\rho U_i)}{\partial U_x}+\frac{\partial(\rho U_j)}{\partial U_y}\right)=0\,. \tag{1}$$

Momentum equation:

$$\frac{DU_j}{Dt}=-\frac{1}{\rho}\frac{\partial p}{\partial x}+\frac{\partial}{\partial x}\left(\upsilon\frac{\partial U_i}{\partial x}\right)+\frac{\partial}{\partial y}\left(\upsilon\frac{\partial U_i}{\partial y}-\overline{u_i u_j}\right) \tag{2a}$$

$$\frac{DU_j}{Dt}=-\frac{1}{\rho}\frac{\partial p}{\partial y}+\frac{\partial}{\partial x}\left(\upsilon\frac{\partial U_j}{\partial x}\right)+\frac{\partial}{\partial y}\left(\upsilon\frac{\partial U_j}{\partial y}\right). \tag{2b}$$

Energy equation:

$$\frac{DT}{Dt}=\frac{\partial}{\partial x}\left(\frac{k}{\rho C_p}\frac{\partial T}{\partial x}-\overline{u_i\theta}\right)+\frac{\partial}{\partial y}\left(\frac{k}{\rho C_p}\frac{\partial T}{\partial y}\right) \tag{3}$$

where U is the velocity, T is the temperature, suffix i and j represents x and y directions, t is the time, D/Dt is the substantial derivative, u is the velocity fluctuations and θ is the temperature fluctuations.

Constant fluid properties are as follows:

p is the pressure, ρ is the density, v is the kinematic viscosity, C_p is the specific heat and k is the thermal conductivity.

The turbulent stresses (Eq. (4)) and the turbulent heat fluxes

(Eq. (5)) are obtained from the Boussinesq and the Fourier relations, respectively:

$$\overline{-u_i u_j} = \upsilon_{tot}\left(\frac{\partial U_i}{\partial x_j}+\frac{\partial U_j}{\partial x_i}\right)-\frac{2}{3}k_{tot}\delta_{ij} \tag{4}$$

$$\overline{-u_i \theta} = \alpha_{\theta,tot}\frac{\partial T}{\partial x_i}. \tag{5}$$

In Eqs. (4) and (5), υ_{tot} and $\alpha_{\theta,tot}$ are the total kinematic eddy viscosity and the total thermal diffusivity, respectively, which accounts for the momentum transport and the thermal energy transport by the large scale and small scale turbulent eddies. k_{tot} is the total turbulent kinetic energy which is obtained by $k_{tot} = k_T + k_L$. Here, k_T and k_L are the turbulent and laminar energy such that $k_T = k_{T,l} + k_{T,s}$ i.e., summation of the large-scale and small-scale energies.

k_T, k_L and ω are obtained from the solution of the collaborative averaged equations that governs their conservation:

$$\frac{Dk_T}{Dt} = Pk_T + R + R_{NAT} - \omega k_T - D_T + \frac{\partial}{\partial x_j}\left[\left(\upsilon+\frac{\alpha_T}{\alpha_k}\right)\frac{\partial k_T}{\partial x_j}\right] \tag{6}$$

$$\frac{Dk_L}{Dt} = Pk_L + R - R_{NAT} - D_L + \frac{\partial}{\partial x_j}\left[\upsilon\frac{\partial k_L}{\partial x_j}\right] \tag{7}$$

$$\frac{D\omega}{Dt} = C_{\omega 1}\frac{\omega}{k_T}P_{k_T} + \left(\frac{C_{\omega R}}{f_\omega}-1\right)\frac{\omega}{k_T}\left(R+R_{NAT}\right) - C_{\omega 2}\omega^2 + C_{\omega 3}f_\omega\alpha_T f_W^2\frac{\sqrt{k_T}}{d^3} + \frac{\partial}{\partial x_j}\left[\left(\upsilon+\frac{\alpha_T}{\alpha_k}\right)\frac{\partial \omega}{\partial x_j}\right]. \tag{8}$$

In the above equations, the rate of production of turbulent kinetic energy by the small-scale turbulent viscosity P_{kT} and the rate of production of laminar kinetic energy by the large-scale turbulent viscosity P_{kL} are obtained by:

$$Pk_T = \upsilon_{T,S}S^2 \tag{9}$$

and

$$Pk_L = \upsilon_{T,l}S^2 \tag{10}$$

where S is the modulus of the mean rate-of-strain tensor.

Near-wall dissipation is given by:

$$D_T = 2\upsilon\frac{\partial\sqrt{k_T}}{\partial x_j}\frac{\partial\sqrt{k_T}}{\partial x_j} \tag{11}$$

$$D_L = 2\upsilon\frac{\partial\sqrt{k_L}}{\partial x_j}\frac{\partial\sqrt{k_L}}{\partial x_j}. \tag{12}$$

R represents the average effect of breakdown of streamwise fluctuations in turbulence during bypass transition, and the

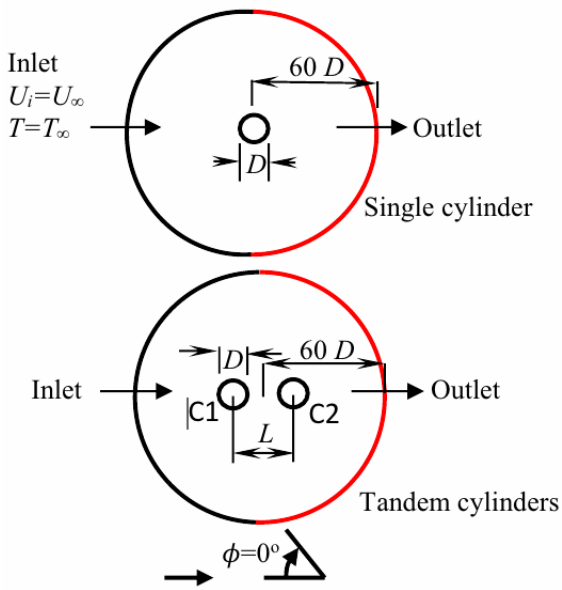

Fig. 1. Layout of computational domain.

R_{NAT} represents the breakdown to turbulence due to instabilities considered as a natural transition production term. The use of ω as the scale-determining variable can lead to a reduced intermittency effect in the outer region of a turbulent boundary layer and consequently an elimination of the wake region in the velocity profile. The various model constants and damping functions may be referred from Ref. [55].

The schematic diagrams of the two-dimensional computational domain for a single and the tandem arrangement of two cylinders are shown in Fig. 1. The cylinder diameter (D) was taken to be 32 mm. The computational domain was 60 times the cylinder diameter from the center provided with only the inlet and the outlet boundaries. The center-to-center distance between the cylinders was L in case of tandem arrangement. The air velocities varied from 5.02 m/s to 18.71 m/s.

Boundary conditions were defined as follows:

At the Inlet: A unidirectional uniform velocity $U_i = U_\infty$ was provided along the x-direction under an ambient condition of $T = T_\infty$.

At the outlet: The outflow boundary condition was used because the flow is fully developed at the outlet boundary.

$$\frac{\partial U_i}{\partial t}+U_i\frac{\partial U_i}{\partial x}=0;\quad \frac{\partial U_j}{\partial t}+U_j\frac{\partial U_j}{\partial x}=0;\quad \frac{\partial T}{\partial t}+U_i\frac{\partial T}{\partial x}=0.$$

At the cylinder wall: A no-slip and a constant-heat-flux condition was given: $U_i = 0$; $U_j = 0$; $q_w = constant$.

2.1 Dimensionless parameters

The dimensionless parameters for the flow field and heat transfer are the drag, lift and pressure coefficients, the Strouhal number and the Nusselt number. The drag, lift and pres-

sure coefficients are defined in Eqs. (13)-(15) where F_x and F_y are the force components along x and y directions. The dimensionless vortex shedding frequency, called as the Strouhal number (St), is obtained from the Power spectral density (PSD) of the time history of fluctuating lift coefficient which is defined by the Eq. (16). The Reynolds number is defined as $Re = \rho U_\infty D/\mu$. The local heat transfer coefficient and the local Nusselt number are computed from Eqs. (17) and (18), respectively, where n denotes the direction normal to the surface and ϕ denotes the angular location at the cylinder surface measured in the clockwise direction with $\phi = 0^o$ being the location of the front stagnation point as shown in Fig. 1. The integration of the local Nusselt number along the cylinder surface provides the average Nusselt number defined in Eq. (19).

$$C_D = \frac{2F_x}{\rho U_\infty^2 D};\quad C_L = \frac{2F_y}{\rho U_\infty^2 D};\quad C_p = \frac{p - p_\infty}{\frac{1}{2}\rho U_\infty^2} \qquad (13, 14, 15)$$

$$S_t = \frac{fD}{U_\infty} \qquad (16)$$

$$h_\phi = \frac{-k\left(\partial T/\partial n\Big|_w\right)}{T_w - T_\infty} \qquad (17)$$

$$Nu_\phi = \frac{h_\phi}{L} \qquad (18)$$

$$Nu_{avg} = \frac{1}{2\pi}\int_{\phi=0}^{\phi=2\pi} Nu_\phi d\phi. \qquad (19)$$

2.2 Simulation procedure and verification

With the flow being incompressible, a pressure-based solver was used in which the velocity field is obtained from the momentum equations. A Green-Gauss theorem was used to compute the gradients and the derivatives of the scalar at the cell center. Pressure discretization utilized the Standard method. Pressure-velocity coupling was achieved by the segregated SIMPLEC algorithm, which is based on the predictor-corrector approach. At each new time step, Eqs. (3)-(12) were solved iteratively until the summation of the normalized residuals of each variable fell below 10^{-4}.

A completely structured O-grid around the cylinders was provided with inlet and outlet boundaries only as shown in Fig. 2. The unsteady flow over cylinders is a complex case because of the separation and reattachment of shear layer and also due to vortex shedding phenomenon. Thus, sensitivity of the mesh resolution has great significance. The complete computational domain was meshed with the quadrilateral elements. A very fine grid was provided close to the cylinder wall which was stretched towards the outer domain. Extensive grid independence tests were performed on a single cylinder based on the number of grid elements, minimum cell distance from the cylinder wall and the time step. For Re = 3.5x10^4 the drag (C_D) and lift (C_L) coefficients, the Strouhal number (S_t) and the average Nusselt number (Nu_{avg}) were obtained, which are tabulated in Table 1. The Strouhal number was obtained from the Fast Fourier transform (FFT) of the time history of lift coefficient, which shows the extent of fluid oscillations.

Table 1. Grid independence on single cylinder: Re = 3.5x10^4.

Case	Grid size	Minimum cell distance	Δt	C_D	C_L	S_t	Nu_{avg}
1	240 x 120	0.00025	10^{-3}	1.46	±1.44	0.163	128.74
2	240 x 120	0.00025	10^{-5}	0.94	±0.005	0.171	142.4
3	300 x 150	0.00025	10^{-3}	1.48	±1.45	0.165	126.8
4	92 x 122	0.01	10^{-5}	1.36	±1.375	0.108	153.57
5	**92 x 122**	**0.0128**	**10^{-5}**	**1.32**	**±1.456**	**0.188**	**154**
6	92 x 122	0.0128	10^{-3}	1.66	±1.62	0.181	135.5
7	92 x 122	0.015	10^{-5}	1.38	±1.46	0.186	154.8

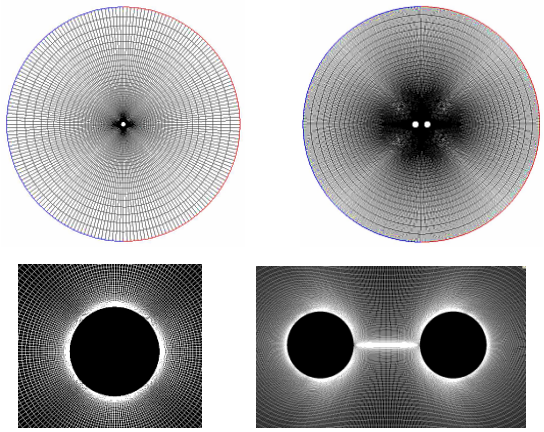

(a) (b)

Fig. 2. Discretization of computational domain and close-up view for (a) single cylinder; (b) tandem cylinders.

The C_D, C_L, S_t and Nu_{avg} were also computed for the Reynolds numbers 1.1x10^4, 2.1x10^4, 3.1x10^4 and 4.1x10^4 and are summarized in Tables 2 and 3. Table 2 depicts the comparative flow field data, whereas Table 3 depicts the heat transfer data from the available experimental and numerical studies.

3. Results and discussion

Table 1 shows three different grid sizes with the minimum cell distance varying between 0.00025D to 0.015D and the time step varying from 10^{-3} to 10^{-5}. The comparison of results with the available results summarized in Tables 2 and 3 reveals that the results of case 5 are better than all the others and are in the acceptable range. The drag coefficient (C_D) is in good consistency with Relf [†], the lift coefficient (C_L) is well within the scatter range of Macovsky [41], the Strouhal number (S_t) is in good agreement with UTIA[†††], and the average Nusselt number (Nu_{avg}) is very close to Perkins and Leppert [43]. The computations involved adopting the time step 10^{-5} on a grid consisting of 92 x 122 nodes and a minimum cell distance of 0.0128D from the cylinder wall. The C_D, C_L, S_t and

Table 2. Comparison C_D, C_L and St of present study with available literature data.

Re	Author	C_D	C_L	S_t
1.1x10^4	Relf (1914)†	1.15	-	-
	DVL Hiebtone (1919)††	-	-	0.192
	UTIA (1955)†††	-	-	0.212
	Igarashi (1981)	-	-	0.219
	Present study	**1.18**	**1.39**	**0.208**
2.1x10^4	Relf (1914)†	1.18	-	-
	DVL Hiebtone (1919)††	-	-	0.202
	Macovsky (1958)	-	1.25±0.5	-
	Igarashi (1981)	-	-	0.205
	Present study	**1.2**	**1.35±0.001**	**0.21**
3.1x10^4	Relf (1914)†	1.34	-	0.192
	Macovsky (1958)	-	1.29±0.5	-
	Igarashi (1981)	-	-	0.204
	Present study	**1.34**	**1.30±0.003**	**0.192**
3.5x10^4	Relf (1914)†	1.3	-	-
	UTIA (1955)†††	-	-	0.185
	Macovsky (1958)	-	1.27±0.5	-
	Igarashi (1981)	-	-	0.203
	Present study	**1.32**	**1.45±0.0031**	**0.188**
4.1x10^4	Relf (1914)†	1.3	-	-
	UTIA (1955)†††	-	-	0.186
	Macovsky (1958)	-	1.21±0.5	-
	Igarashi (1981)	-	-	0.203
	Present study	**1.34**	**1.36±0.002**	**0.1902**

†, ††, †††: Data refers to Fig. 5. 30 pp121 of Zdravkovich [2].

Nu_{avg} at all the Reynolds number 1.1x10^4, 2.1x10^4, 3.1x10^4 and 4.1x10^4 are also consistent with the available results summarized in Tables 2 and 3, which further validates the simulation procedure.

3.1 Flow past single cylinder

Fig. 3 illustrates the comparison of computational results of the distributions of pressure coefficient (C_p) over the cylinder at various Reynolds numbers from 1.1x10^4 to 4.1x10^4 with the available literature by Dong et al. [53], Yokuda et al. [47], Linke [40], Igarashi [22] and Tsutsui and Igarashi [29]. A good agreement of the C_p with the available literature data is obtained from the front stagnation point till the point of separation (ϕ = 73°). However, a close agreement in the C_p is observed with small deviations after the separation in each case, which may be attributed to the three-dimensional effect of the flow field. The mean deviation of these discrepancies is 2.7 %.

Fig. 4 shows the local Nusselt number distributions over the cylinder by varying the Reynolds number from 1.1x10^4 to 4.1x10^4 and are compared with the available experimental data of Tsutsui and Igarashi [29]. These data of Tsutsui and Igarashi [29] were represented at 10 % blockage and the aspect ratio of 3.75, which were 14 % higher than that of Igarashi and Hirata [46] who did not consider the blockage and aspect ratio. The computed values of the Nusselt number under the present study, in which the blockage and the aspect ratios were not considered, show a good agreement on the front side of the cylinder and are consistent with the minimum values at the respective Reynolds number compared to the reported values data of Tsutsui and Igarashi [29]. However, little higher values of the Nusselt number were obtained on the rear side of the cylinder in the present computations. The deviation could be due to the round-off errors during the numerical solution.

Table 3. Comparison of Nu_{avg} of present study with available literature.

Re	Author	Nu_{avg}
1.1x10^4	Igarashi and Harita	68
	Perkins and Leppert	78
	Goldstein	62
	Present study	**69**
2.1x10^4	Igarashi and Harita	97
	Perkins and Leppert	117
	Goldstein	97.5
	Present study	**101.06**
3.1x10^4	Igarashi and Harita	121.5
	Perkins and Leppert	146.5
	Goldstein	127
	Present study	**144**
3.5x10^4	Igarashi and Harita	133
	Perkins and Leppert	156
	Goldstein	136
	Present study	**154**
4.1x10^4	Igarashi and Harita	145
	Perkins and Leppert	170.5
	Goldstein	150
	Present study	**151**

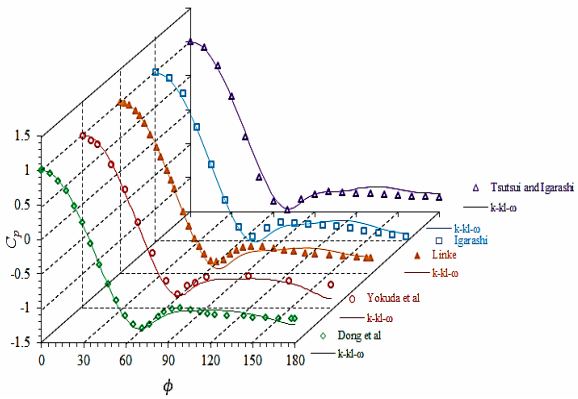

Fig. 3. Comparison of distribution of pressure coefficients for single cylinder with available literature (◇Re = 1.1x10^4 [53], oRe = 2.1x10^4 [47], ▲Re = 3.1x10^4 [40], □Re = 3.5x10^4 [22], △Re = 4.1x10^4 [29]).

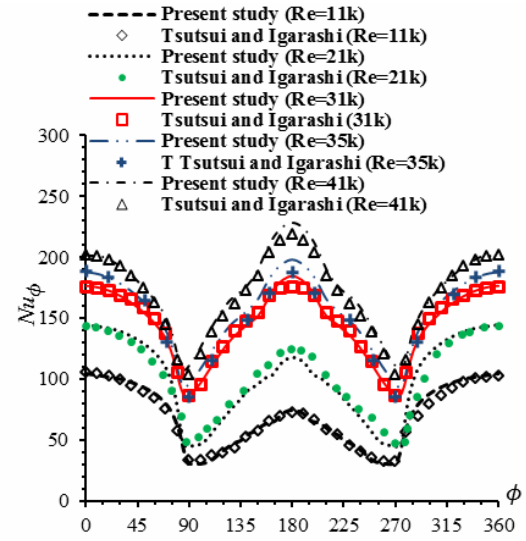

Fig. 4. Local Nusselt number obtained in present study and comparison with available experimental results at Reynolds number from $1.1x10^4$ to $4.1x10^4$ for single cylinder.

Figs. 5(a)-(c) show the distribution of time-averaged Nusselt number normalized with the Reynolds number, the r.m.s. distribution of Nusselt number fluctuations normalized with the Reynolds number and the instantaneous vorticity contours, respectively. A comparison of the local Nusselt number fluctuations of the present study with that of Scholten and Murray [49] and Nakamura and Igarashi [52] is presented in Fig. 5(b). On the front side of the cylinder in the laminar boundary layer region ($\phi < 65^o$), the normalized time averaged Nusselt number is the same for all the Reynolds numbers. In this region, a negligible fluctuation in the Nusselt number persists as observed from Fig. 5(b). In region-1 around the separation point ($\phi = 65^o$-85^o) as shown in Fig. 5(c), a hump indicates a disturbance created by a Small-scale vortex (SSV) ahead of the separation point. The SSV sweeps the low velocity particles over the surface in region-2, resulting in low heat transfer. The fluctuation in the Nusselt number increases, as the SSV moves forward till it detaches from the surface ($85^o < \phi < 110^o$). During this movement of SSV the flow particles sweep the surface with increasing velocity, which increases the Nusselt number. The rise in the Nusselt number is more apparently visible at higher Reynolds numbers ($Re > 2.1x10^4$). The SSV detaches under the force of another Large-scale vortex (LSV) coming from the opposite side of the cylinder. Thus, a region-3 is created where the movements of the flow particles are very small, which results in a slow growth in the Nusselt number and a flatness in its fluctuation ($110^o < \phi < 135^o$). Further, in the separated flow region, an increase in the Nusselt number was obtained together with the intensification of fluctuations in the Nusselt number after $\phi = 135^o$ till the rear stagnation point ($\phi = 180^o$), which is attributed due to a high frequency of vortex shedding (shown in the region-4 in Fig. 5(c)). Fig. 5(b) also depicts the increase of fluctuations in Nusselt number with increase in Reynolds number in the separated flow region. Comparing the r.m.s. distribution of Nusselt number fluctuations normalized with the Reynolds number with the results of Scholten and Murray [49] and Nakamura and Igarashi [52], the present computation provides similar results with a small deviation in region-3.

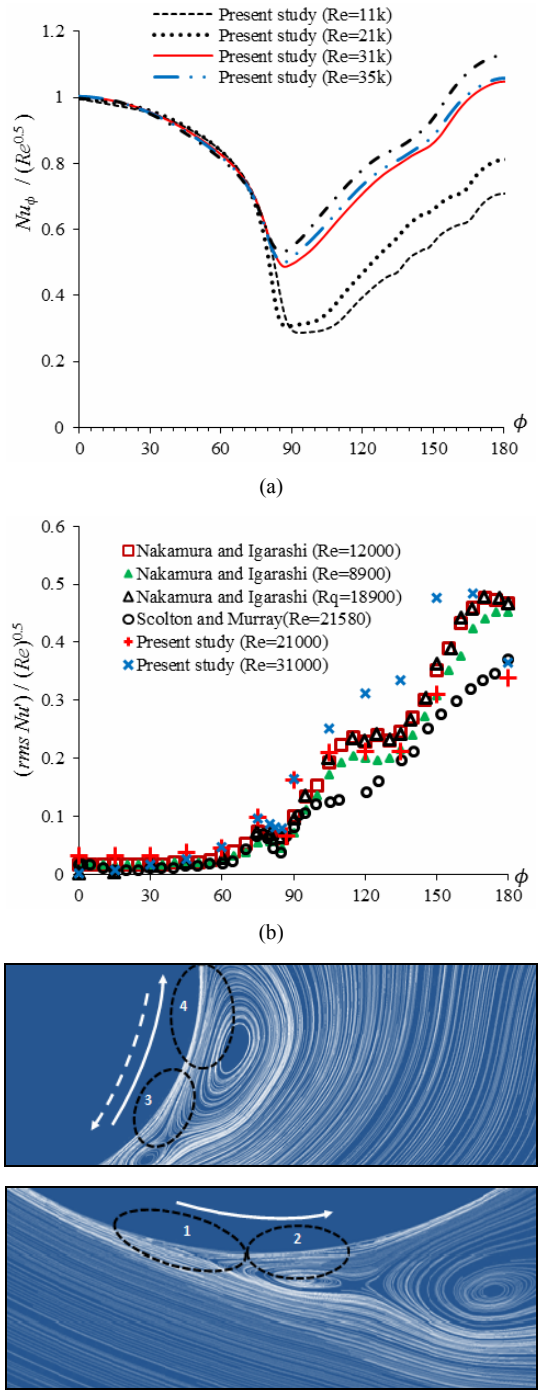

Fig. 5. (a) Time-averaged local Nusselt number normalized with Reynolds number; (b) comparison of local Nusselt number fluctuations of present study with available literature; (c) instantaneous vorticity contours obtained at $Re = 3.5x10^4$.

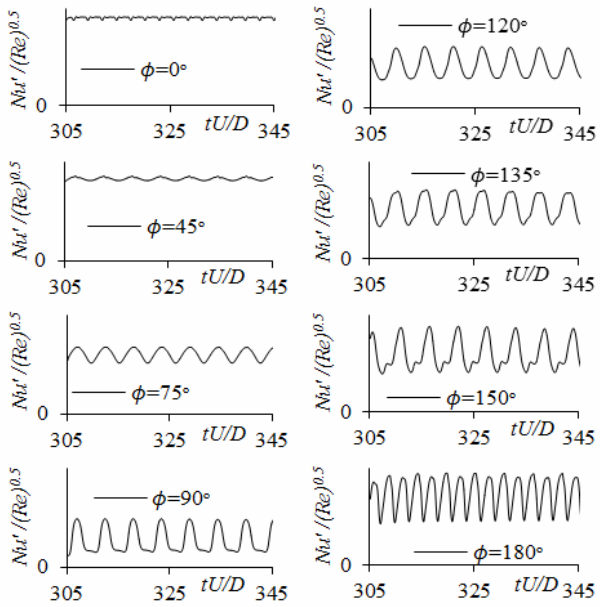

(a) Local Nusselt number fluctuations normalized with Reynolds number at $Re = 2.1x10^4$

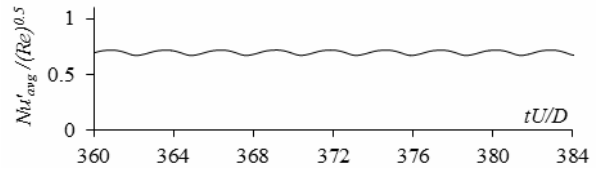

(b) Average Nusselt number fluctuations normalized with Reynolds number at $Re = 2.1x10^4$

Fig. 6. Time history of local and average Nusselt number fluctuations for single cylinder.

Fig. 6(a) shows the time traces of the fluctuations in local Nusselt number normalized with the Reynolds number, which may be simultaneously compared with the Figs. 5(a)-(c). Insignificant fluctuations in the Nusselt number with higher time average value at $\phi = 0^o$ and with relatively lower time average value at $\phi = 45^o$ represents the region-1. $\phi = 75^o$ represents the region-2 where the amplitude of Nusselt number fluctuations is higher with relatively lower time average value. $\phi = 90^o$ represents the region between 85^o-110^o where the Nusselt number fluctuations are relatively higher with very low time average value. $\phi = 120^o$ and 135^o lies in the region-3 where the amplitudes of fluctuations are same with very small increase in the time average value of the fluctuating Nusselt number. $\phi = 150^o$ and 180^o lies in the region-4 where the time average value of fluctuating Nusselt number as well as the amplitude of fluctuations increases with increase in the angular location till the rear stagnation point. The time traces of fluctuating average Nusselt number, as shown in Fig. 6(b), depicts that the amplitude of average Nusselt number fluctuations is small.

Fig. 7 compares the average Nusselt number (Nu_{avg}) of the single cylinder with respect to the Reynolds number with the correlation suggested by Perkins and Leppert [43], Fand [44],

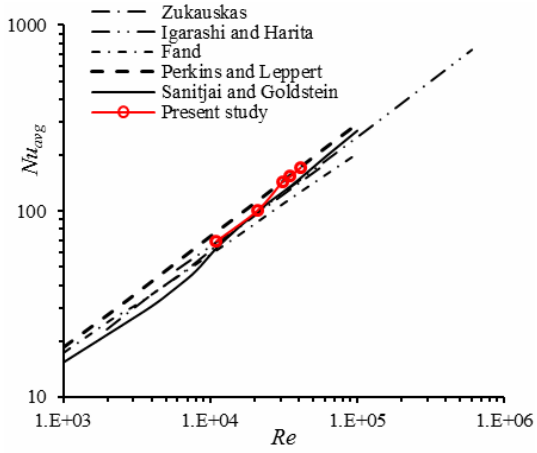

Fig. 7. Comparison of Nu_{avg} of single cylinder based on Reynolds number.

Zukauskas [45], Igarashi and Hirata [46] and Sanitjai and Goldstein [51]. Although at $Re > 2.1x10^4$, the Nu_{avg} is slightly on the higher side compared to the majority of the authors, but lies well within the reported range of their respective work. We attribute the higher values of Nu_{avg} due to the round-off errors during the numerical computations. Also, the present simulation procedure depicts a transition between the Reynolds numbers of $2.1x10^4$ and $3.1x10^4$ on the log-log plot. Out of all the compared literatures, only Sanitjai and Goldstein [51] observed a transition between the Reynolds numbers $5x10^3$ to 10^4. The lower range of Reynolds number in the transition by Sanitjai and Goldstein [51] may be due to the common conclusions of their experiments conducted in air as well as the various liquid mixtures of compositions of water and ethylene glycol by considering the Prandtl number (Pr) of the compositions.

3.2 Flow past two tandem cylinders at variable spacing

After obtaining results on single cylinder, the two cylinders placed in tandem were investigated by adopting a similar computational scheme. The size of the computational domain as well as the solution procedure for simulation was kept the same as in the case of single cylinder. During the grid independence test, the number of cells varied from 15000 to 90000, while the minimum cell distance of 0.0128D from the cylinder wall was kept the same. Finally, 304 nodes were created on each cylinder wall forming a grid size of (304+304)x125. Thus, the computational domain was discretized into 76000 quadrilateral cells. The simulations were under a constant-heat-flux condition for $Re = 2.1x10^4$ and $Re = 3.5x10^4$. The spacing ratios (L/D) between the cylinders varied from 1.2 to 4.0, for which the drag and lift coefficients were monitored.

For the validation of the simulation scheme the distribution of pressure coefficient at $Re = 3.5x10^4$ for L/D ratios 1.18, 1.9, 3.0 and 4.0 was obtained over both the cylinders and compared with the C_p experimentally obtained by Igarashi [22]. A uniform decrease of C_p on the front portion of upstream cylin-

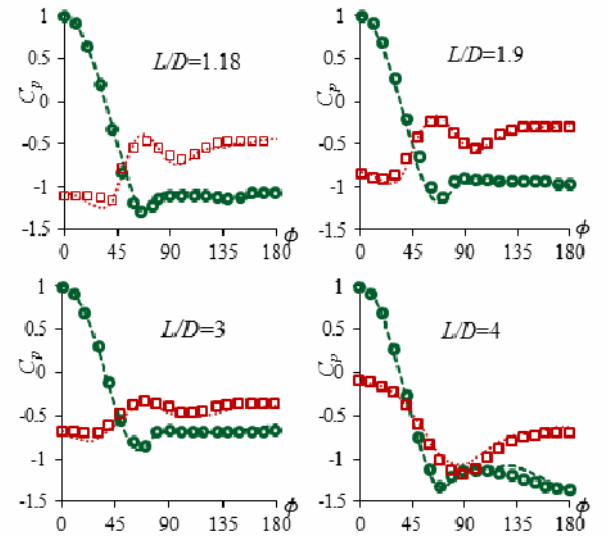

Fig. 8. Comparison of C_p distribution on upstream and downstream cylinders of present study with Igarashi [22] at $Re = 3.5x10^4$ for L/D = 1.18, 1.9, 3.0 and 4.0 (c1-upstream cylinder; c2-downstream cylinder) [○c1-Igarashi; □c2-Igarashi; - - - - c1-present study; •••• c2-present study].

der, existence of the separation point, flatness on the rear portion for $L/D \leqslant 3$, reattachment of the shear layer, a smooth decrease after the reattachment of shear layer at $L/D = 4.0$ and the base pressure coefficient were obtained in good agreement with that of Igarashi [22] as shown in Fig. 8. In case of downstream cylinder, the C_p at the front stagnation point matches well with that of Igarashi [22]. However, a slight difference in the C_p values was observed around $\phi = 30^o$ and 60^o for $L/D \leqslant 3$ and after $\phi = 60^o$ for $L/D = 4.0$. A smooth decrease of C_p on the front portion of the upstream cylinder and then the attainment of minimum value around $\phi = 70^o$ shows a laminar growth of boundary layer followed by the flow separation. The flatness in the C_p distribution and its identical values at the rear stagnation point of upstream cylinder and the front stagnation point of downstream cylinder indicates the presence of quasi-stationary vortices between the two cylinders. A peak at around $\phi = 100^o$ on the upstream cylinder for L/D = 4.0 and at around $\phi = 65^o$ on the downstream cylinder for $L/D \leqslant 3$ indicates the reattachment of shear layer separated from the upstream cylinder. Also, Fig. 9 has been plotted to compare the C_p obtained in the present computational work at $Re = 2.1x10^4$ with that of the experimental study of Ljungkrona et al. [48] at $Re = 2x10^4$ and the computational study of Kitagawa and Ohto [54] at $Re = 2.2x10^4$ for $L/D = 2.0$, 3.0 and 4.0. The C_p distribution obtained from the present computations agrees well in almost all the cases with Ljungkrona et al. [48] and Kitagawa and Ohto [54] except on the rear portion of downstream cylinder for $L/D = 2.0$, where significant lower values were observed with respect to that of Ljungkrona et al. [48]. The C_p obtained by Kitagawa and Ohto [54] on the rear potion highly deviated with respect to that of Ljungkrona et al. [48]. From the figure, the computational height has a signifi-

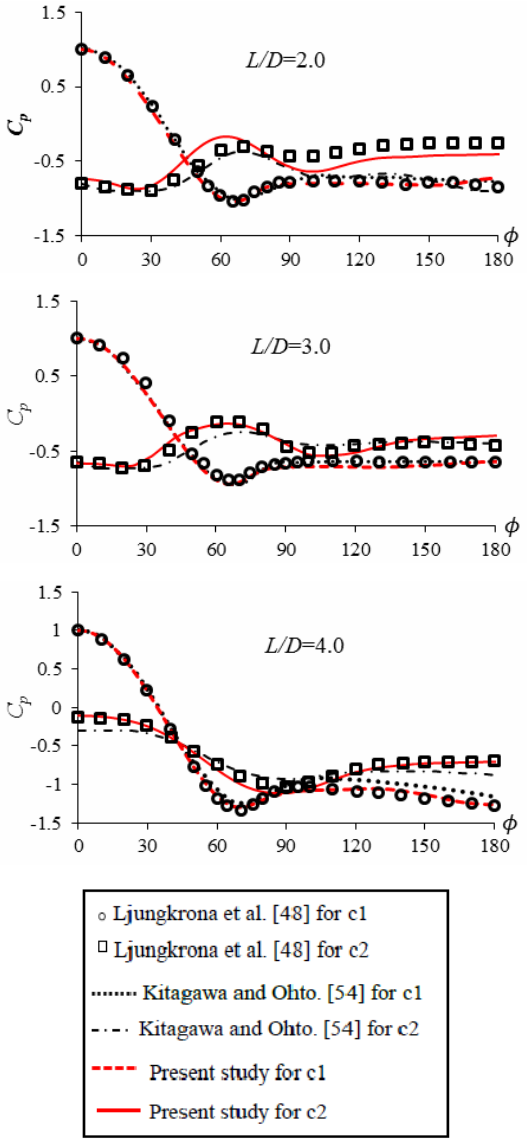

Fig. 9. Comparison of C_p distribution on upstream and downstream cylinders of present study $Re = 2.1x10^4$ with Ljungkrona et al. [48] at $Re = 2x10^4$ and Kitagawa et al. [54] at $Re = 2.2x10^4$ for L/D = 2.0, 3.0 and 4.0 (c1-upstream cylinder; c2-downstream cylinder).

cant effect on C_p distribution only on the rear side of the downstream cylinder for $L/D < 3.0$ with respect to the work of Kitagawa and Ohto [54], which was a three-dimensional computational study at $Re = 2.2x10^4$ and Ljungkrona et al. [48], which was a two-dimensional experimental study at $Re = 2x10^4$.

Figs. 10 and 11 show the instantaneous vorticity and pathlines, at $Re = 3.5x10^4$ for various L/D ratios from 1.2 to 4.0. These figures show that for every spacing ratio, a laminar boundary layer forms on the front portion of the upstream cylinder followed by separation nearby $\phi = 70^o$. Until L/D = 3.0, the separated shear layer from the upstream cylinder reattaches nearby $\phi = 60^o$- 65^o. As observed from Figs. 10(a) and 11(a)-(c) that for $L/D \leqslant 1.8$, a pair of quasi-stationary vortices

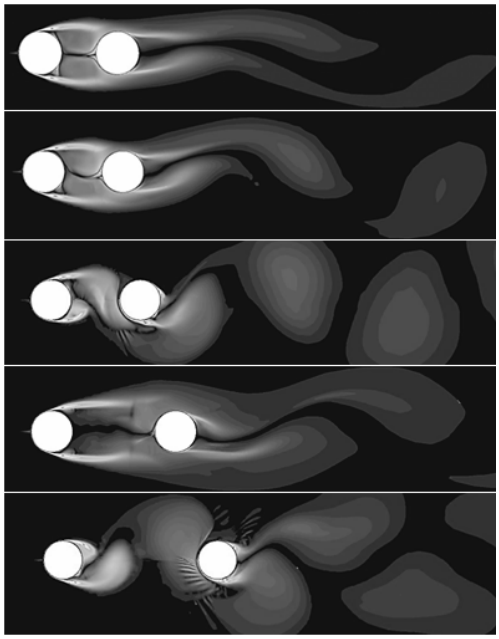

Fig. 10. Instantaneous vorticity contours at Re = 3.5x10^4 for various spacing ratios.

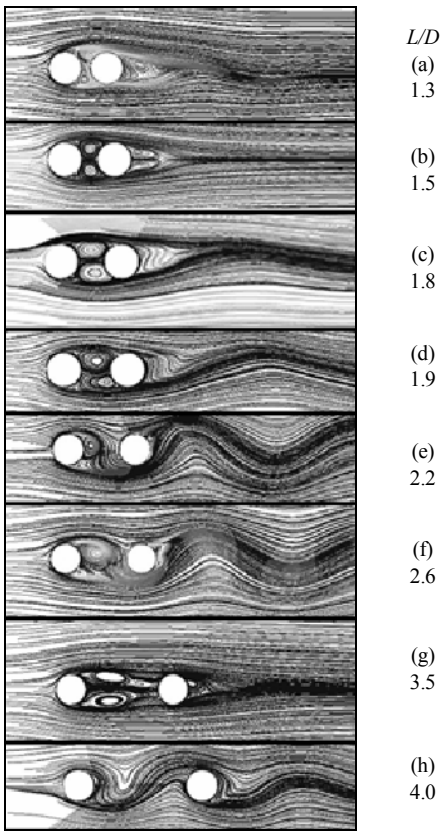

Fig. 11. Instantaneous pathlines at Re = 3.5x10^4.

establishes contact with both the cylinders in the interference region, while a low velocity circulation is observed near the rear stagnation point of the upstream cylinder and the front stagnation point of the downstream cylinder. The shear layer after the reattachment on downstream cylinder flows along its surface towards the front stagnation point as well as the rear stagnation point on the downstream side. The shear layer on the downstream side re-separates nearby ϕ = 135^o and results in the shedding of vortices behind the downstream cylinder. From Figs. 10(b), (c), 11(d) and (e), the quasi-stationary vortices become unstable at L/D = 1.9, while at L/D = 2.2 the separate vortices start shedding from the upstream cylinder in the interference region. As seen from Figs. 10(c), (d), 11(e) and (f), although the separate vortices shed from the upstream cylinder, the shear layer still impinges on the downstream cylinder near ϕ = 60^o-65^o. After L/D = 3.0, the reattachment point of shear layer starts to move towards the front stagnation point of the downstream cylinder. At L/D = 4.0, a complete vortex with integral separated shear layer from the upstream cylinder impinges on the downstream cylinder as illustrated in Figs. 10(e), 11(g) and (h). Thus, the flow past the downstream is like a single cylinder with the vortices of high magnitude to shed behind it.

Fig. 12 shows the time histories of lift and drag coefficients for the spacing ratios L/D = 1.4, 1.8, 2.2 and 4.0 at Re = 3.5x10^4 where c1 and c2 refer to the upstream and the downstream cylinders, respectively. From the figures, the drag coefficient on the upstream cylinder ($C_{D,1}$) reduces by placing another cylinder behind it. The reduction in the $C_{D,1}$ is due to the increase of low pressure on its downstream side because of the presence of downstream cylinder. The $C_{D,1}$ increases and tends to approach the C_D of single cylinder by increasing the spacing ratio between the cylinders. For L/D < 3.5, the drag coefficient on downstream cylinder ($C_{D,2}$) is negative due to the effect of low pressure wake of the upstream cylinder. For L/D < 1.8, the fluctuations of $C_{D,1}$ and $C_{D,2}$ have very small amplitudes with non-uniform oscillations, whereas the lift coefficient of upstream cylinder ($C_{L,1}$) has relatively larger amplitude compared to the lift coefficient of downstream cylinder ($C_{L,2}$). However, these amplitudes are so small that the forces acting on both the cylinders produce no significant effect. Oscillations of $C_{D,1}$ and $C_{D,2}$ are due to the combined effect of the reattachment of shear layer from the upstream cylinder as well as the shedding of vortices behind the downstream cylinder with low frequency and strength as also depicted from Figs. 10, 11 and 16. Non-uniformity in oscillations results from the interference effect, which leads to the variations in the shear layer thickness as well as its movement from the upstream cylinder. For $L/D \geqslant$ 1.8, uniformity in both the fluctuating drag and lift coefficients has been observed with amplitude increasing with the L/D ratio. The increase in amplitude is observed till L/D = 2.2 and thereafter it becomes constant till L/D = 4.0.

The plots of $C_{L,1}$ and $C_{L,2}$ imply that the amplitude of fluctuations of $C_{L,1}$ is more than that of $C_{L,2}$ at L/D = 1.4. However, they become almost the same at L/D = 1.8, while at L/D = 2.2 the amplitude of $C_{L,2}$ becomes more than that of $C_{L,1}$. This may be due to the application of forces on the upstream cylinder because of the combined effect of forces produced by the

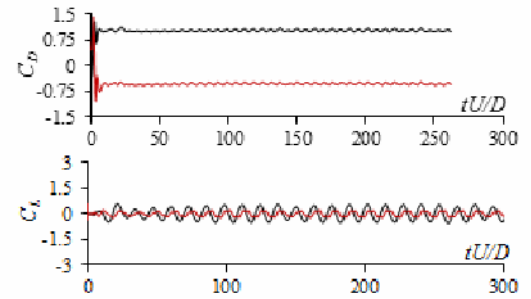

(a) C_d and C_L at L/D = 1.4

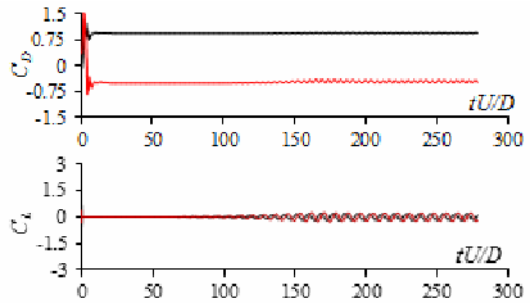

(b) C_d and C_L at L/D = 1.8

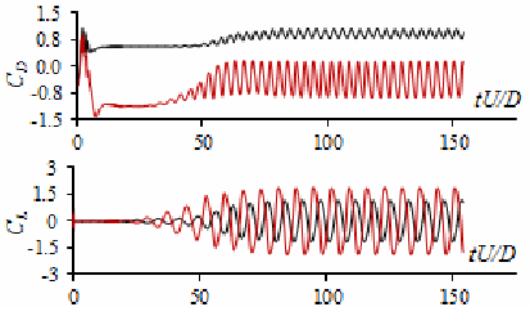

(c) C_d and C_L at L/D = 2.2

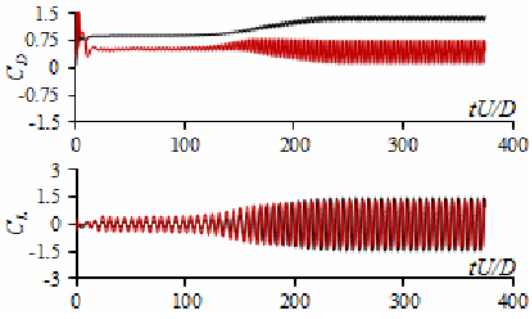

(d) C_d and C_L at L/D = 4.0

Fig. 12. Time history of drag (upper) and lift (lower) coefficients at Re = 3.5x10^4 at L/D = 1.4, 1.8, 2.2, 4.0 (— c1; — c2).

separation of shear layer and the shedding of vortices behind the downstream cylinder. These forces shift from the upstream cylinder to the downstream cylinder with increase in the spacing ratio. At L/D = 4.0, it was observed that the amplitude of $C_{L,2}$ remained same as that in case of L/D = 2.2, while the amplitude of $C_{L,1}$ approached that of $C_{L,2}$. Under this spacing ratio the vortex along with the separated shear layer from the

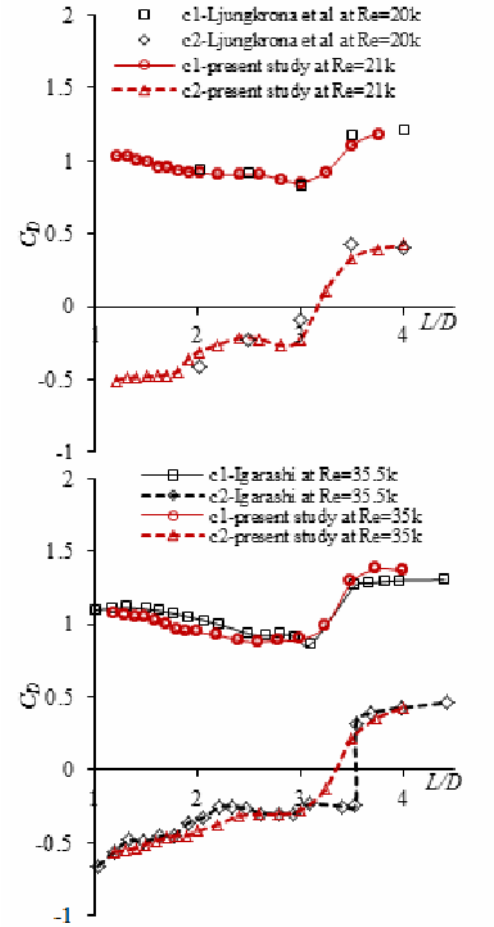

Fig. 13. Drag coefficient (C_D) of upstream and downstream cylinder for 1.2 ⩽ L/D ⩽ 4.0 at Re = 2.1x10^4 and 3.5x10^4 (c1-upstream cylinder; c2-downstream cylinder).

upstream cylinder directly impinged on the downstream cylinder as shown in Fig. 10(e). The combined effect of the impinged vortices on the downstream cylinder from the upstream cylinder and the vortices that shed behind the downstream cylinder increases the drag force and its amplitude of fluctuation over the downstream cylinder.

The mean drag coefficients (C_D) of both the upstream and the downstream cylinders at Re = 2.1x10^4 and 3.5x10^4 for spacing ratios 1.2 < L/D < 4.0 are shown in Fig. 13. Consistent with the results of Ljungkrona et al. [48] and Igarashi [22], with the increase in L/D ratio the C_D of the upstream cylinder decreases, while for the downstream cylinder it increases till the critical value ($C_{D,C}$). The $C_{D,C}$ of upstream cylinder is obtained when it achieves a minimum positive, while for the downstream cylinder it is obtained when the C_D changes from negative to positive. The $C_{D,C}$ for upstream cylinder is obtained at L/D = 3, which is the same as reported by Ljungkrona et al. [48] and Igarashi [22]. Beyond this value, it increases sharply. However, we obtained a constant C_D between 2.6 < L/D < 3.0 at Re = 3.5x10^4, whereas the C_D decreases continuously to attain a minimum value at L/D = 3.0, which shows that with change in Reynolds number, the $C_{D,C}$

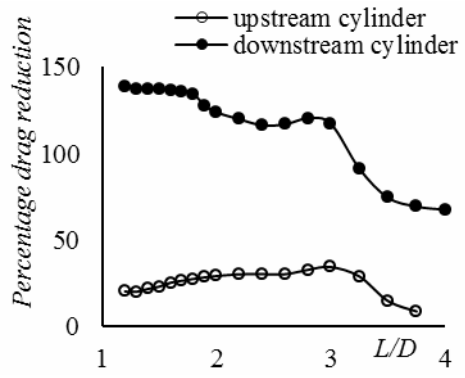

(a)

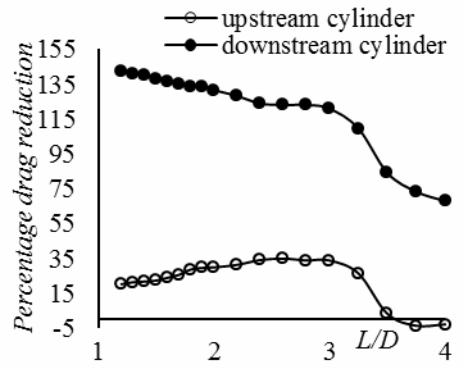

(b)

Fig. 14. (a) Percentage reduction in drag coefficient with respect to single cylinder for $Re = 2.1\text{x}10^4$; (b) percentage reduction in drag coefficient with respect to single cylinder for $Re = 3.5\text{x}10^4$.

gradually shifts relative to the L/D ratio. The C_D for the downstream cylinder has crowning with peak at $L/D = 2.5$ before the critical value. The $C_{D,C}$ was obtained between $L/D = 3$ and 3.25 for $Re = 2.1\text{x}10^4$ and between $L/D = 3.25$ and 3.5 for $Re = 3.5\text{x}10^4$. Thus, in the case of downstream cylinder also the $C_{D,C}$ has dependency on the Reynolds number. For $Re = 3.5\text{x}10^4$, the C_D obtained from the present study is slightly on the lower side because the calculations of Igarashi [22] are based on the integration of pressure distribution only. However, in the present computation the C_D was obtained due to the combined effect of pressure and fluid friction forces.

Figs. 14 (a) and (b) illustrate the percentage reduction in C_D for the upstream and downstream cylinders with respect to the single cylinder for Reynolds numbers $2.1\text{x}10^4$ and $3.5\text{x}10^4$. From the figure, when a cylinder is placed behind a single cylinder the C_D of the cylinder which is at the upstream location undergoes a reduction in its value. The percentage drag reduction increases with the increase in L/D ratio and it becomes almost constant for L/D in the range of 2.2-3.0. After $L/D = 3.0$, the percentage reduction in C_D decreases and becomes equivalent to that of the single cylinder for $L/D \geqslant 3.5$. The C_D on the front side of the downstream cylinder is negative because of the suction pressure created in front of the downstream cylinder, which increases with increase in L/D ratio as depicted in Fig. 13 as well. Thus, the percentage reduction in C_D, which is very high with respect to the single cylinder, decreases with the increase in L/D ratio. Likewise, the upstream cylinder as in the case of downstream cylinder also, the percentage reduction in drag becomes almost constant for L/D in the range of 2.2-3.0. However, after $L/D = 3.0$, the percentage reduction in C_D decreases further with increase in the L/D ratio.

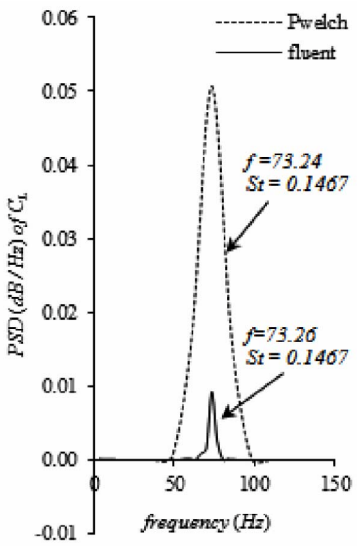

(a) L/D = 2.2 at Re = 3.5×10^4

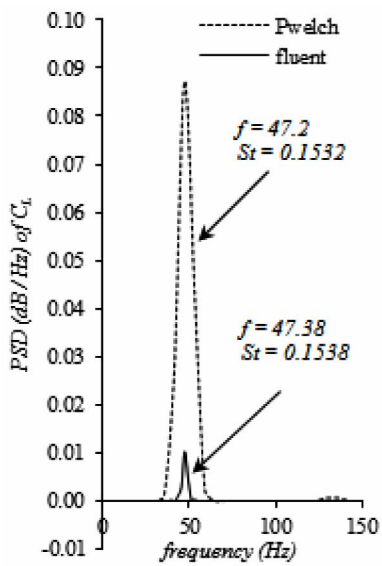

(b) L/D = 2.2 at Re = 2.1×10^4

Fig. 15. Comparison of power spectral density between Fluent and Pwelch method.

Power spectrum analysis was carried out at $L/D = 2.2$ for $Re = 2.1\text{x}10^4$ and $3.5\text{x}10^4$ by using Pwelch method of Matlab as well as the post processing facility of the Fluent. Fig. 15 shows the comparison of Power spectral density (PSD) of the lift coefficient of downstream cylinder obtained by the post processing of Fluent with that of obtained by Pwelch method. From both the figures (a) and (b), it is evident that the domi-

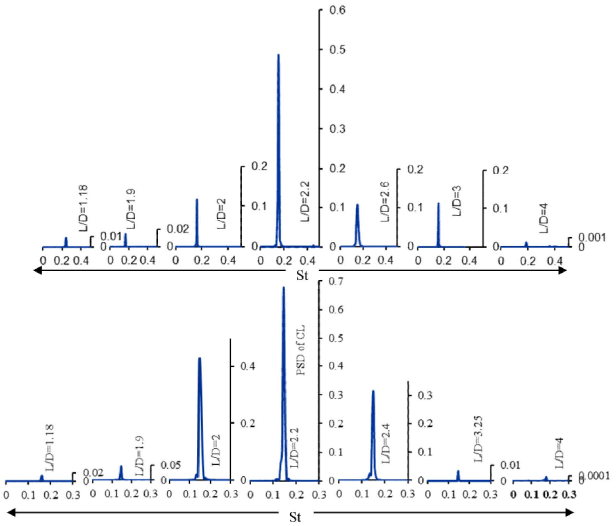

Fig. 16. Power spectral density of lift coefficient obtained on downstream cylinder for $Re = 2.1x10^4$ (Upper) and $Re = 3.5x10^4$ (lower).

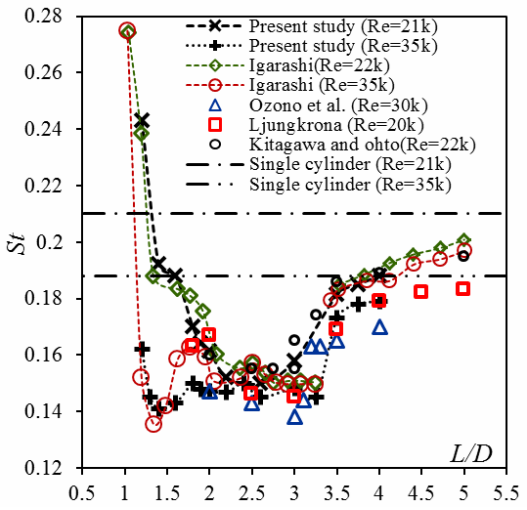

Fig. 17. Strouhal number obtained by FFT of C_L on downstream cylinder.

nating frequencies of the vortex shedding that corresponds to Strouhal number obtained by both the methods are almost the same. Thus, the post processing of Fluent was used with 99.9 % confidence for the spectrum analysis.

The Strouhal number (St) was obtained from the Fast Fourier transformation (FFT) of the time history of lift coefficient (C_L) observed on the downstream cylinder for $Re = 2.1x10^4$ and $Re = 3.5x10^4$ as shown in Fig. 16. The maximum peak indicates the Strouhal number corresponding to the main shedding frequency. The strength of vortex shedding can be determined from the time history of C_L. The figure also shows clear and distinct vortex streets obtained at L/D ratios from 2.0-3.0. Out of this range of L/D ratio the vortices are irregular and unstable. The comparison of St of the present study for the two Reynolds numbers $2.1x10^4$ and $3.5x10^4$ and spacing ratios $1.2 \leqslant L/D \leqslant 4.0$ with the St reported by Igarashi [22], Ljungkrona et al. [48], Ozono et al. [50] and Kitagawa and Ohto [54] is shown in Fig. 17. The figure shows a strong dependency of Reynolds number as well as the spacing ratio of the two cylinders. The St obtained from the present study, Igarashi [22] and Kitagawa and Ohto [54] are in close agreement with each other although some discrepancies were seen for the L/D ratios between 1.5-2.0. This may be attributed to a highly irregular and unstable flow in this range of L/D ratio which was also reported by Igarashi [22]. For the L/D ratio between 2.0 and 3.0 the St of all the literatures are in close proximity and their average provides a $St = 0.151$ showing less dependency on the Reynolds number. Within this range of L/D ratio the vortex streets are clear and distinct behind the downstream cylinder. At L/D ratio between 3.0 and 3.3, various authors observed a sudden jump in the St and obtained two distinct values because of the shedding of vortex from the upstream cylinder and an intermittent jump phenomenon as mentioned by Igarashi [22], which we could not obtain from the present study. Beyond this jump phenomenon, the St smoothly increases to approach the St for single cylinder, which is the same as obtained in other literatures.

Fig. 18 shows the Nusselt number distribution over the upstream and the downstream cylinders at $Re = 3.5x10^4$ by varying the spacing ratio from 1.2 to 4.0. As depicted from Fig. 18(a) for the upstream cylinder, the distribution of the Nusselt number over the front portion ($\phi < 80^o$) of the cylinder is the same for all the L/D ratios. Over this portion the Nusselt number smoothly decreases starting from the front stagnation point due to a smooth growth of laminar boundary layer which acts as a resistance to heat flow. Although the flow separation takes place at around $\phi = 70^o$ as depicted in Fig. 8, the minimum Nusselt number was obtained in the proximity of $\phi = 85^o$. This was because of the reverse flow ahead of the separation point and the detachment of Small-scale vortex (SSV) from the cylinder surface as shown in Fig. 11. The minimum Nusselt number is greatly dependent on the spacing between the cylinders. Ahead of the minimum value, the Nusselt number increases till the rear stagnation point ($\phi = 180^o$) behind the cylinder for all the L/D ratios. However, a drop in the Nusselt number with a second minimum value was observed for $L/D < 2.0$, which occurs due to the presence of the quasi-stationary vortices between the cylinders as depicted in the Figs. 10(a) and 11(a)-(d). After $L/D = 1.8$, the quasi-stationary vortices become unstable as shown in Figs. 10(b)-(e) and thus a rise in the Nusselt number takes place in a manner as that of the single cylinder till the rear stagnation point.

The distribution of the Nusselt number over the downstream cylinder, as shown in Fig. 18(b), reveals that the shear layer from the upstream cylinder strikes on it at $\phi = 60^o$- 65^o yielding a peak result in high heat transfer rate. Referring to the Figs. 10(a)-(d), the fluid from this location undergoes an attached flow on both the directions towards the front as well as the rear stagnation points of the downstream cylinder. Because of the attached flow, the Nusselt number decreases on

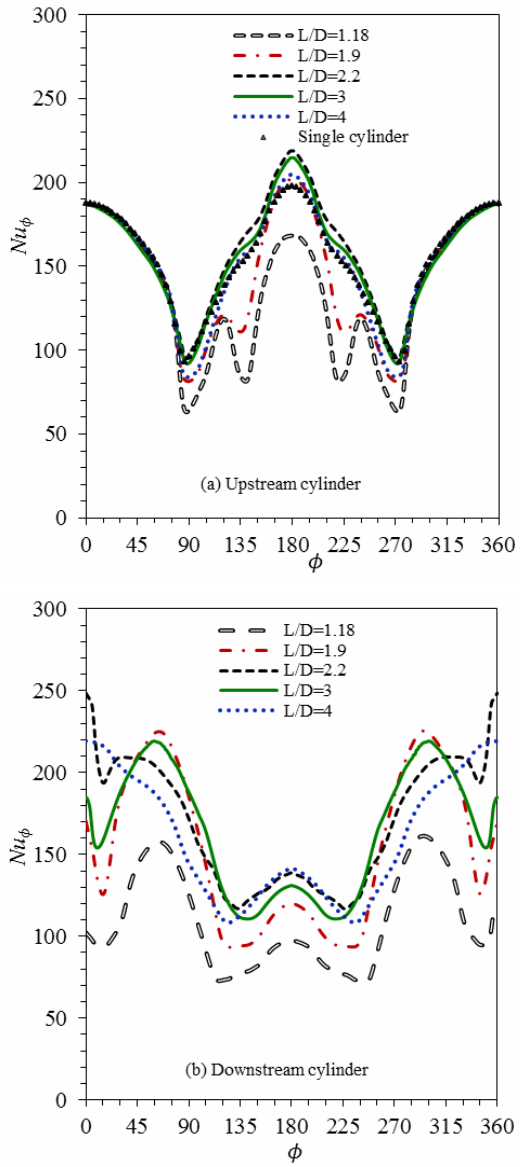

Fig. 18. Comparison of Nusselt number distribution of tandem cylinders based on L/D ratio at $Re = 3.5\text{x}10^4$.

both the directions and attains the minimum values adjacent to $\phi = 5^o$ and 135^o. As shown in Figs. 10(a), (b) and 11(a)-(d), in the region between $\phi = \pm 5^o$ adjacent to front stagnation point, there always exists a narrow circulation zone of low flow velocity also shown in Fig. 19(a) where a small increase in the heat transfer was observed. Similarly, in the region between $\phi = \pm 135^o$ about rear stagnation point the re-separation of shear layer near 135^o produces a recirculation zone as shown in Fig. 19(b), but due to the low flow velocity, low heat transfer has been observed in this region. For $L/D > 3.0$, the vortices from the upstream cylinder impinged over the downstream cylinder as shown in Fig. 10(e) and the flow field and heat transfer over the downstream cylinder is like single cylinder with separation near 135^o.

The average Nusselt numbers (Nu_{avg}) of the upstream and

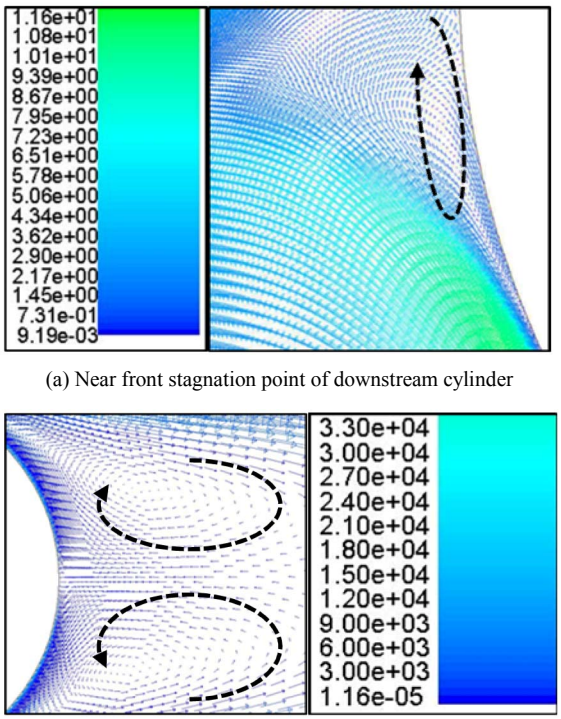

(a) Near front stagnation point of downstream cylinder

(b) Behind the downstream cylinder

Fig. 19. Instantaneous velocity vectors at $L/D = 1.8$ and $Re = 3.5\text{x}10^4$.

the downstream cylinders for L/D ratios from 1.2 to 4.0 at $Re = 2.1\text{x}10^4$ and $3.5\text{x}10^4$ are plotted in Fig. 20. The overall average Nusselt number of both the cylinders is also presented in the figure. The data clearly follows that the Nu_{avg} increases with increase in the Reynolds number. It is observed that the Nu_{avg} of the downstream cylinder is always more than that of the upstream cylinder. This observation is different from that of Mihir and Altac [18], who conducted studies on tandem cylinder at $Re = 100$ and 200. A close observation reveals that at lower Reynolds number $2.1\text{x}10^4$ and for small ($L/D < 2$) and large ($L/D > 3$) spacing ratios, the Nu_{avg} of downstream cylinder is less than that of the upstream cylinder. This indicates that if we decrease the Reynolds number the Nu_{avg} may approach the observations made by Mihir and Altac [18]. From this observation, it may be concluded that for the higher subcritical range of Reynolds number, the downstream cylinder acts as the heat promoter, especially between the L/D ratios of 2.0 and 3.0. Also from the figure, the Nu_{avg} increases with increase in the spacing ratio and attains a maximum value at $L/D = 2.2$, and thereafter it decreases. It undergoes insignificant change for $L/D \geqslant 3.5$, and thus reveals that the flow interference is effective on heat transfer for the spacing ratios less than 3.5. A curve was plotted as shown in Fig. 21, obtaining the overall Nu_{avg} for $L/D = 2.2$, which is the spacing ratio for maximum heat transfer rate under the CHF condition for various Reynolds numbers from $1.1\text{x}10^4$ to $6.2\text{x}10^4$. The results were compared with the Nu_{avg} of a single cylinder for these Reynolds numbers obtained under the CHF condition. Thus, at the spacing ratio of 2.2, the overall Nu_{avg} of the two

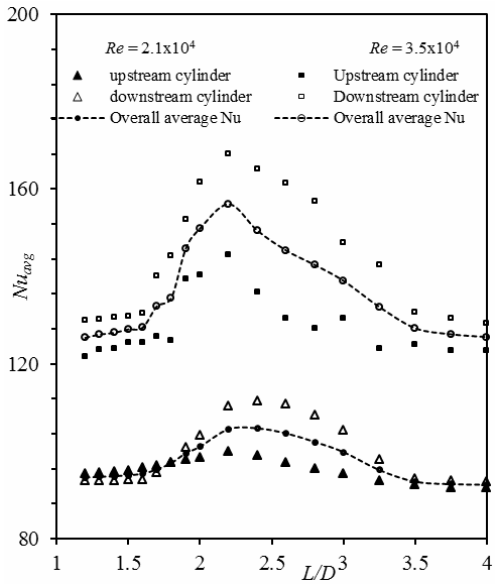

Fig. 20. Comparison of average Nusselt number on two tandem cylinders at $Re = 2.1\text{x}10^4$ and $3.5\text{x}10^4$.

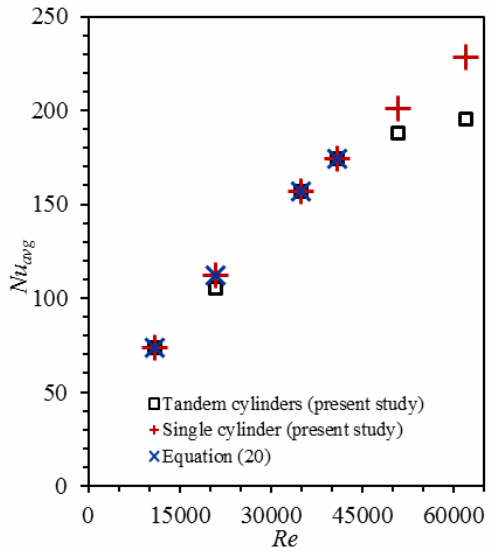

Fig. 21. Comparison Nu_{avg} of two tandem cylinders at $L/D = 2.2$ and that of single cylinder with respect to Reynolds number.

tandem cylinders are comparable with that of single cylinder within the Reynolds number range from $1.1\text{x}10^4$ to $4.1\text{x}10^4$ illustrating that if the two cylinders are placed at the spacing of 2.2 their combination can produce heat transfer twice that of the single cylinder. After $Re = 4.1\text{x}10^4$, the overall Nu_{avg} is quite lower than that of the single cylinder, which indicates that for the Reynolds number higher than $4.1\text{x}10^4$ the L/D ratio may be different for a comparable or a higher heat transfer rate than that of a single cylinder.

Eq. (20) has been proposed for the prediction of overall Nu_{avg} under the CHF condition at the cylinder surface of the two tandem cylinders placed at $L/D = 2.2$, which is a spacing ratio for the maximum heat transfer rate for a range of Reynolds number $1.1\text{x}10^4 \leqslant Re \leqslant 4.1\text{x}10^4$ in cross-flow of air.

$$\text{Overall } Nu_{avg} = 0.182\,(Re)^{0.6568}\,(Pr)^{0.33}. \quad (20)$$

Using $Pr = 0.71$ for the air under ambient condition, the Eq. (20) is modified as:

$$\text{Overall } Nu_{avg} = 0.1626(Re)^{0.6568}. \quad (21)$$

4. Conclusions

Unsteady simulations for the flow field and convective heat transfer were carried out on a single cylinder and the two tandem cylinders of same diameter subjected to cross-flow of air using a commercial software FLUENT®. The computations were carried out in a two-dimensional domain using a 3-equation k-kl-ω turbulence model. The flow and the energy governing equations were solved for the constant-heat-flux conditions at the cylinder surfaces under the subcritical range of Reynolds number from $1.1\text{x}10^4$ to $4.1\text{x}10^4$. The spacing between the tandem cylinders varied from 1.2 to 4.0 times the cylinder diameter. A reasonably good agreement in the comparison of flow field and heat transfer parameters with the available literatures establishes the favorable capabilities of the k-kl-ω turbulence model in the domain of heat and fluid flow past the bluff bodies. It is observed that the coefficients of forces (C_p, C_D and C_L), Strouhal number and the wake structure are strongly dependent on the spacing between the cylinders. The mean drag coefficient and the Strouhal number undergo insignificant change between the L/D ratios 2.0 and 3.0 for the considered Reynolds numbers $2.1\text{x}10^4$ and $3.5\text{x}10^4$. The study of Strouhal number, the vorticity contours and the pathlines indicates that between L/D ratio 2.0 and 3.0, the vortex streets are clear and distinct behind the downstream cylinder and show less dependency on the Reynolds number.

The study of local Nusselt fluctuations reveals that the instability behind the cylinder leads to an increase of heat transfer providing the flow particles must sweep the surface. Analogous to flow parameters, the Nusselt number also showed a dependency on L/D ratio and the Reynolds number. For higher rates of heat transfer the L/D ratio should be such that the separated shear layer from the upstream cylinder must impinge on the downstream cylinder. For the higher subcritical Reynolds number, the downstream cylinder is identified as the heat promoter especially between the L/D ratios of 2.0 and 3.0. It is observed that the overall heat transfer from the two tandem cylinders attains a maximum value at $L/D = 2.2$, and the interference is effective on heat transfer for a spacing ratio less than 3.5. Thus, from the flow field and heat transfer observation, it is concluded that $L/D = 2.2$ is the critical spacing ratio for collective consideration of the heat and fluid flow.

A new correlation in terms of Reynolds number has been proposed based on the present investigation to estimate the overall average Nusselt number under the CHF condition at

the critical spacing ratio of L/D = 2.2 for the two tandem cylinders.

References

[1] B. M. Sumer, *Hydrodynamics around cylindrical structures*, World Scientific, Singapore (1997).

[2] M. M. Zdravkovich, *Flow around circular cylinders, vol 1: fundamentals*, Oxford U. Press, London (1997).

[3] M. M. Zdravkovich, *Flow around circular cylinders, vol 2: applications*, Oxford U. Press, London (2003).

[4] R. J. Goldstein, W. E. Ibele, S. V. Patankar, T. W. Simon, T. H. Kuehn, P. J. Strykowski, K. K. Tamma, J. V. R. Heberlein, J. H. Davidson, J. Bischof, F. A. Kulacki, U. Kortshagen, S. Garrick, V. Srinivasan, K. Ghosh and R. Mittal, Heat Transfer-A review of 2005 literature, *Int. J. of Heat and Mass Transfer*, 53 (2010) 4397-4447.

[5] A. Kondjoyan and H. C. Boisson, Comparison of calculated and experimental heat transfer coefficients at the surface of circular cylinders placed in a turbulent cross-flow of air, *J. of Food Engineering*, 34 (1997) 123-143.

[6] K. Szczepanik, A. Ooi, L. Aye and G. Rosengarten, A numerical study of heat transfer from a cylinder in cross flow, *Proc. of 15th Australasian Fluid Mechanics Conference*, Sydney, Australia (2004).

[7] B. A. Younis, M. C. Banica and B. Weigand, Prediction of vortex shedding with heat transfer, *Numerical Heat Transfer, Part A*, 48 (2005) 1-19.

[8] Md. M. Rahman, Md. M. Karim and Md. A. Alim, Numerical investigation of unsteady flow past a circular cylinder using 2-d finite volume method, *J. of Naval Architecture and Marine Engineering*, 4 (2007) 27-42.

[9] S. Mittal, V. Kumar and A. Raghuvanshi, Unsteady incompressible flows past two cylinders in tandem and staggered arrangements, *Int. J. for Numerical Methods in Fluids*, 25 (1997) 1315-1344.

[10] J. R. Meneghini, F. Saltara, C. L. R. Siqueira and J. A. Ferrari Jr., Numerical simulation of flow interference between two circular cylinders in tandem and side-by-side arrangements, *J. of Fluids and Structures*, 15 (2001) 327-350.

[11] W. Jester and Y. Kallinderis, Numerical study of incompressible flow about fixed cylinder pairs, *J. of Fluids and Structures*, 17 (2003) 561-577.

[12] B. S. Carmo, J. R. Meneghini and S. J. Sherwin, Secondary instabilities in the flow around two circular cylinders in tandem, *J. of Fluid Mech.*, 644 (2010) 395-431.

[13] R. Jiang, J. Lin and X. Ku, Numerical predictions of flows past two tandem cylinders of different diameters under unconfined and confined flows, *Fluid Dyn. Res.*, 46 (2014) 1-22.

[14] H. Chen, Z. Zheng, Z. Chen and T. B. Xiaotao, Simulation of flow and heat transfer around a heated stationary circular cylinder by lattice gas automata, *Powder Technology*, 290 (2016) 72-82.

[15] S. U. Islam and C. Y. Zhou, Numerical simulation of flow around a row of circular cylinders using the lattice Boltzmann method, *Information Technology Journal*, 8 (2009) 513-520.

[16] S. U. Islam, C. Y. Zhou and A. Farooq, Numerical simulations of cross-flow around four square cylinders in an in-line rectangular configuration, *Int. J. of Mechanical, Aerospace, Industrial, Mechatronic and Manufacturing Engineering*, 3 (9) (2009) 1138-1147.

[17] G. Juncu, A numerical study of momentum and forced convection heat transfer around two tandem circular cylinders at low Reynolds numbers Part II: Forced convection heat transfer, *Int. J. of Heat and Mass Transfer*, 50 (2007) 3799-3808.

[18] N. Mahir and Z. Altac, Numerical investigation of convective heat transfer in unsteady flow past two cylinders in tandem arrangements, *Int. J. of Heat and Fluid Flow*, 29 (2009) 1309-1318.

[19] S. Jayawel and S. Tiwari, Numerical investigation of incompressible flow past circular tubes in confined channel, *CFD Letters,* 1 (1) (2009) 1-14.

[20] I. Harimi and M. Saghafian, Numerical simulation of fluid flow and forced convection heat transfer from tandem circular cylinders using overset grid method, *J. of Fluids and Structures*, 28 (2012) 309-327.

[21] D. Lee, J. Ahn and S. Shin, Uneven longitudinal pitch effect on tube bank heat transfer in cross flow, *Applied Thermal Engineering*, 51 (2013) 937-947.

[22] T. Igarashi, Characteristics of flow around two circular cylinders arranged in tandem, *Bulletin of JSME*, 24 (188) (1981) 323-331.

[23] Md. M. Alam, M. Moriya, K. Takai and H. Sakamoto, Fluctuating fluid forces acting on two circular cylinders in a tandem arrangement at a subcritical Reynolds number, *J. Wind Eng. Ind. Aerodyn.*, 91 (2003) 139-154.

[24] T. Kitagawa and H. Ohta, Numerical investigation on flow around circular cylinders in tandem arrangement at a subcritical Reynolds number, *J. of Fluids and Structures*, 24 (2008) 680-699.

[25] Z. G. Kostic and S. N. Oka, Fluid flow and heat transfer with two cylinders in cross flow, *Int. J. of Heat and Mass Transfer*, 15 (2) (1972) 279-282.

[26] T. Igarashi and H. Yamasaki, Fluid flow and transfer around two circular cylinders arranged in tandem, *Proc. of 2nd JSME-KSME Thermal Engineering Conf.* (1992) 7-12.

[27] E. Buyruk, Heat transfer and flow structures around circular cylinders in cross-flow, *Tr. J. Engineering and Environmental Science*, 23 (1999) 299-315.

[28] A. Daloglu and A. Unal, Heat Transfer from a cylinder in wake flow, *Int. Comm. Heat Mass Transfer*, 27 (4) (2000) 569-580.

[29] T. Tsutsui and T. Igarashi, Heat transfer enhancement of a circular cylinder, *ASME J. Heat Transfer*, 128 (2006) 226-233.

[30] J. H. Lin, C. -K. Chen and Y.-T. Yang, An inverse method for simultaneous estimation of the center and surface thermal

behavior of a heated cylinder normal to a turbulent air stream, *ASME J. Heat Transfer*, 124 (2002) 601-608.

[31] E. Coment, T. Loulou and D. Maillet, Estimation of local heat transfer coefficient on a cylinder: comparison between an analytical and an optimization method, *Inverse Problems in Science and Engineering*, 13 (5) (2005) 449-467.

[32] C.-K. Chen, L.-W. Wu and Y.-T. Yang, Application of the inverse method to the estimation of heat flux and temperature on the external surface in laminar pipe flow, *Appl. Therm. Eng.*, 26 (2006) 1714-1724.

[33] H.-T. Chen, J. C. Chou and H. C. Wang, Estimation of heat transfer coefficient on a vertical plate fin of finned-tube heat exchangers for various air speeds and fin spacing, *Int. J. Heat Mass Transfer*, 50 (2007) 45-57.

[34] H.-T. Chen and W.-L. Hsu, Estimation of heat transfer coefficient on the fin of annular finned-tube heat exchangers in natural convection for various fin spacings, *Int. J. Heat Mass Transfer*, 50 (2007) 1750-1761.

[35] H.-T. Chen and W.-L. Hsu, Estimation of heat transfer characteristics on a vertical annular circular fin of finned-tube heat exchangers in forced convection, *Int. J. Heat Mass Transfer*, 51 (2008) 1920-1932.

[36] J. Taler, Determination of local heat transfer coefficient from the solution of the inverse heat conduction problem, *Forsch Ingenieurwes*, 71 (2007) 69-78.

[37] E. E. M. Olsson, H. Janestad, L. M. Ahrne, A. C. Tragardh and R. P. Singh, Determination of local heat-transfer coefficients around a circular cylinder under an impinging air jet, *Int. J. of Food Properties*, 11 (2008) 600-612.

[38] A. H. Benmachiche, C. Bougriou and S. Abboudi, Inverse determination of the heat transfer characteristics on a circular plane fin in a finned-tube bundle, *Int. J. of Heat Mass Transfer*, 46 (2010) 1367-1377.

[39] W. L. Chen, Estimation of heat flux on the surface of an initially hot cylinder cooled by a laminar confined impinging jet, *Int. J. of Heat and Mass Transfer*, 55 (2012) 597-606.

[40] W. Linke, New measurements on aerodynamics of cylinders particularly their friction resistance (in German), *Physikalische Zeitschrift*, 38 (1931) 476-98 (Courtesy: [2]).

[41] M. S. Macovsky, *Vortex-Induced vibration studies*, Report No. 1190, Navy Department, David Tayler Model Basin, Hydromechanics Laboratory, July (1958).

[42] H. C. Perkins and G. Leppert, Forced convection heat transfer from a uniformly heated cylinder, *J. of Heat Transfer*, 84 (1962) 257-263.

[43] H. C. Perkins and G. Leppert, Local heat-transfer coefficients on a uniformly heated cylinder, *Int. J. Heat Mass Transfer*, 7 (1964) 143-158.

[44] R. M. Fand, Heat transfer by forced convection from a cylinder to water in crossflow, *Int. J. of Heat Mass Transfer*, 8 (1965) 995-1010.

[45] A. A. Zukauskas, Heat transfer from tubes in cross-flow, *Adv. Heat Transfer*, 8 (1972) 93-160.

[46] T. Igarashi and M. Hirata, Heat transfer in separated flows Part 2: Theoretical Analysis, *Heat Transfer-Jpn Res.*, 6 (3) (1977) 60-78.

[47] S. Yokuda and B. R. Ramaprian, The dynamics of flow around a cylinder at subcritical Reynolds numbers, *Phys. Fluids A*, 2 (5) (1990) 784-791.

[48] L. Ljungkrona, C. H. Norberg and B. Sunde´n, Free-stream turbulence and tube spacing effects on surface pressure fluctuations for two tubes in an in-line arrangement, *J. of Fluids and Structures*, 5 (1991) 701-727.

[49] J. W. Scholten and D. B. Murray, Unsteady heat transfer and velocity of a cylinder in cross flow- I. Low free stream turbulence, *In. J. Heat Mass Transfer*, 41 (100) (1998) 1139-1148.

[50] S. Ozono, J. Oda, Y. Yoshida and Y. Wakasugi, Critical nature of the base pressure of the upstream circular cylinder in two staggered ones in cross-flow, *Theoretical and Applied Mechanics*, 50 (2001) 335-340.

[51] S. Sanitjai and R. J. Goldstein, Heat transfer from a circular cylinder to mixtures of water and ethylene glycol, *Int. J. Heat Mass Transfer*, 47 (2004) 4795-4805.

[52] H. Nakamura and T. Igarashi, Unsteady heat transfer from a circular cylinder for Reynolds numbers from 3000 to 15,000, *Int. J. of Heat and Fluid Flow*, 25 (2004) 741-748.

[53] S. Dong, G. E. Karniadakis, A. Ekmekci and D. Rockwell, A combined direct numerical simulation-particle image velocimetry study of the turbulent near wake, *J. Fluid Mech.*, 569 (2006) 185-207.

[54] T. Kitagawa and H. Ohta, Numerical investigation on flow around circular cylinders in tandem arrangement at a sub-critical Reynolds number, *J. of Fluids and Structures*, 24 (2008) 680-699.

[55] ANSYS, Inc., *Fluent 14.0, ANSYSFLUENT Theory Guide*, (2011).

S. K. Dhiman received his B.E. in Mechanical Engineering, Government Engineering College, Rani Durgavati University, Jabalpur (India) and M.Tech. in Thermal Engineering, Maulana Azad National Institute of Technology, Bhopal (India). He is an Assistant Professor of Mechanical Engineering at Birla Institute of Technology, Mesra, Ranchi (India). His principal domain of research is fluid mechanics and heat transfer.